ACS APPLIED MATERIALS & INTERFACES

Research Article

www.acsami.org

Tailoring the Electrical Properties of Graphene Layers by Molecular Doping

Arun Kumar Singh,[†] Muneer Ahmad,[‡] Vivek Kumar Singh,[§] Koo Shin,[§] Yongho Seo,[‡] and Jonghwa Eom*[,†]

[†]Department of Physics and Graphene Research Institute, Sejong University, Seoul 143-747, Korea

[‡]Faculty of Nanotechnology and Advanced Materials, HMC, and Graphene Research Institute, Sejong University, Seoul 143-747, Korea

[§]Department of Chemistry and Graphene Research Institute, Sejong University, Seoul 143-747, Korea

ABSTRACT: It is an essential issue in graphene-based nanoelectronic and optoelectronic devices to tune the electrical properties of graphene layers, while preserving its unique band structure. Here, we report the tuning of electronic properties of single-, bi-, and trilayer mechanically exfoliated graphenes by *p*-toluenesulfonic acid (PTSA) molecular doping. Raman spectroscopy and charge transport measurements revealed that PTSA molecule imposes *n*-doping to single-, bi-, and trilayer graphenes. The shift of G and 2D peak frequencies and intensity ratio of single-, bi-, and trilayer graphenes are analyzed as a function of reaction time. The Dirac point is also analyzed as a function of reaction time indicates the *n*-type doping effect for all single-, bi-, and trilayer graphenes. Our study demonstrates that chemical modification is a simple approach to tailor the electrical properties of single-, bi-, and trilayer graphenes, while maintaining the important electrical assets.

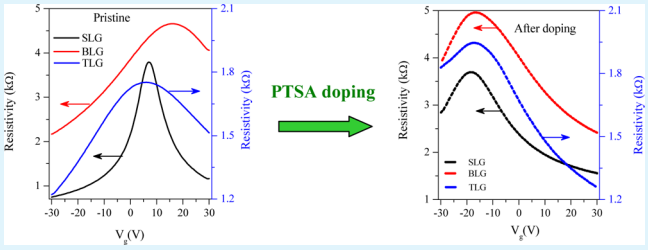

KEYWORDS: *graphene, molecular doping, electrical properties, Raman spectroscopy, transparent conducting electrode*

1. INTRODUCTION

Recently, graphene is attractive as an important material for transparent conducting electrodes in many modern optoelectronic devices, such as touch screens, liquid crystal displays (LCDs), organic light emitting diodes (OLEDs), and solar cells, all of which are growing in demand.[1−3] Graphene's perfect two-dimensional carbon crystalline structure enables not only unprecedented exploration of fundamental physics but also the exciting potential applications in postsilicon nanoelectronics.[4] Graphene also possesses remarkable high charge carrier mobility at room temperature, high optical transmittance, and flexibility in very low manufacturing cost, and these properties made graphene an ideal candidate for a transparent conducting electrode (TCE).[5−8] High transparency and flexibility are very important parameters for a material to be used as TCE in flexible optoelectronics.[8,9] Although indium tin oxide (ITO) has been used as a TCE in many optoelectronic devices, ITO (a ceramic material) suffered from many disadvantages, including increased material costs, costs associated with vacuum deposition, poor transparency in the blue and near-infrared light ranges, instability in the presence of acids or bases, and brittleness making it unsuitable for flexible substrates.[1,10−12]

The tuning of electrical properties of graphene is very important for successful operation of the optoelectronic devices based on it. Several methods like depositing the dopant atoms,[13] absorption of gas molecules,[14] or by aromatic compounds[15−18] and electrostatic field tuning have been applied to modulate the electronic properties of graphene.[19] However, chemical doping is one of the most effective methods to tailor the electrical properties of graphene. It is because of their unique ability to adapt the electronic structure of graphene. The absorbed molecules form covalent or noncovalent chemical bonds to graphene surface and usually form the stable structure. The covalent attachment of chemical species changes the basic electronic structure of graphene and potentially reduce the charge carrier mobility.[20] However, noncovalent attachment of chemical species with graphene not only tunes electronic properties of graphene but also minimizes the damage to carbon lattice.[20] This type of chemical doping is effective, simple and significant way to tailor the electronic properties of graphene, while preserving its unique band structure as we reported for chemical vapor deposited single layer graphene by molecular doping.[21]

Another important theme in recent graphene-based research is to tailor the electrical properties of graphene as a function of the layer number because different graphene layers have different electronic structure.[22] For example, the electronic structure of trilayer graphene (TLG) is distinct from bilayer graphene (BLG), and electronic structure of BLG is distinct from that of single-layer graphene (SLG). It is already reported

Received: March 28, 2013
Accepted: May 15, 2013
Published: May 15, 2013

   dx.doi.org/10.1021/am401119j | ACS Appl. Mater. Interfaces 2013, 5, 5276−5281

that some inorganic materials, such as Au, Ag, Br, or I, induce different doping effects for SLG, BLG, and TLG because the layer number of graphene affects the morphology of the metals deposited on graphenes.[13] The study of different graphene layers is also important for TCE because stacking of graphene layers reduces the sheet resistance, which is the main hurdle for graphene used as TCE in electronic devices[23−25] The optical absorption of graphene layers varies linearly proportional to the number of layers and each layer absorb 2.3% in the visible region.[7] However, up to three layers graphene still have sufficient transparency (>90%).

Here we report the tailoring of electronic properties of single-, bi-, and trilayer mechanically exfoliated graphenes by *p*-toluenesulfonic acid (PTSA) molecular doping without significantly degrading its electrical properties. Raman spectroscopy and charge transport measurements revealed that PTSA molecule imposes n-doping for all single-, bi-, and trilayer graphenes. The charge neutrality point for single-, bi-, and trilayer graphenes is also analyzed as a function of reaction time. It is found that the Dirac point is shifted toward negative gate voltage with increase in reaction time for all single-, bi-, and trilayer graphenes. The results indicate that chemical modification is a simple approach to tailor the electrical properties of single-, bi-, and trilayer graphenes, while maintaining the electrical properties.

2. EXPERIMENTAL SECTION

2.1. Preparation of Graphenes. The SLG, BLG, and TLG films were obtained by mechanical exfoliation of natural graphite flakes by using the adhesive tape and then transferred onto a Si/SiO_2 wafer. The layer numbers of the graphene films were identified by optical microscope and Raman spectroscopy as shown in Figure 1. The big patterned electrodes (Cr/Au of 5/30 nm) for all SLG, BLG, and TLG were made by photolithography on Si/SiO_2 substrate. Fine electrodes for charge neutrality point measurements were made by e-beam lithography and evaporation of Cr/Au (6/50 nm). The device structures of SLG, TLG, and BLG are shown in Figure 1a and b, respectively.

2.2. PTSA Doping and Characterization. The modification of graphene properties by PTSA was investigated by transport measurements, Raman spectroscopy, and atomic force microscopy. The gate voltage dependent resistivity measurements and Raman spectroscopy were performed on the same device before and after different duration of PTSA treatment for all SLG, BLG, and TLG samples. The *p*-toluenesulfonic acid monohydrate (ACS reagent, ≥98.5%) was obtained from Aldrich and dissolved in deionized water to make the concentration of 0.1 M solution. Raman spectra were collected at room temperature with a Renishaw microspectrometer over wavenumber from 1100 to 3200 cm^{-1} with the laser wavelength of 514 nm. To avoid local heating and the introduction of defects due to the laser, the laser power was kept at ∼1.0 mW. The SLG, BLG, and TLG on the Si/SiO_2 substrate were soaked in the PTSA solution for certain period of time and dried with nitrogen gas. Further, we put the sample in vacuum desiccator for 1 day to completely dry the samples. For Dirac point measurements, we used the 4-terminal method and device was measured using a standard lock-in amplifier technique at room temperature in vacuum. The surface morphology of pristine SLG, BLG, and TLG and PTSA-doped SLG, BLG, and TLG were also characterized by using commercial atomic force microscope (Nano-Focus Inc.).

3. RESULTS AND DISCUSSION

The optical microscope images of the SLG and TLG device are shown in Figure 1a and that of BLG device fabricated on SiO_2/Si substrate is shown in Figure 1b. The SLG, BLG, and TLG were identified on the basis of their optical contrast, and here,

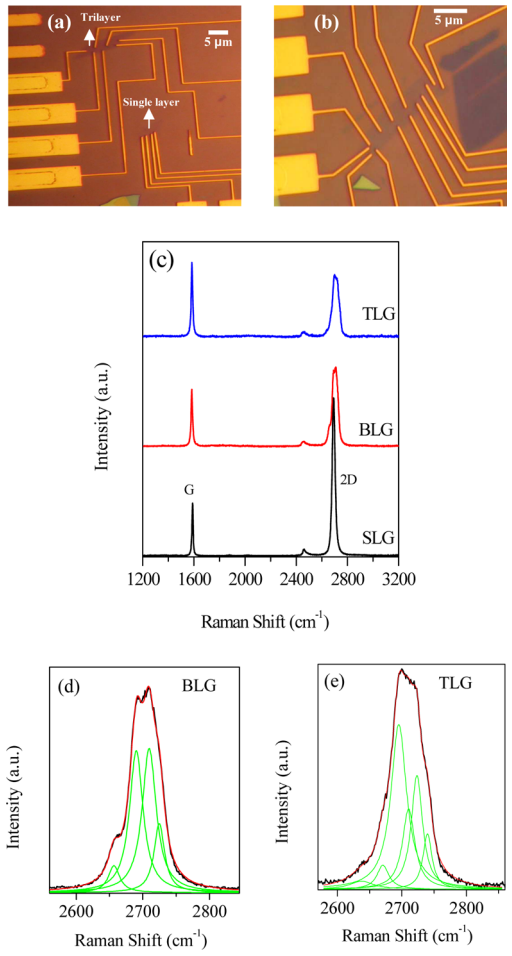

Figure 1. Optical microscopy image of (a) single- and trilayer and (b) bilayer devices and (c) Raman spectra of pristine single-, bi-, and trilayer graphene. Lorenz curve fitting of 2D peak of (d) bilayer and (e) trilayer graphene.

we can clearly see the different optical contrast for different graphene layers as shown in Figure 1a and b. The numbers of graphene layers were further confirmed by Raman spectroscopy. Figure 1c shows the Raman spectra of pristine SLG, BLG, and TLG. The characteristic G and 2D peaks for pristine SLG appears around 1589 and 2692 cm^{-1}, respectively, and the ratio of I_{2D}/I_G is found to be 3.3 for pristine SLG, which is also the signature of single layer graphene. The characteristic G and 2D peaks for pristine BLG appears around 1584 and 2701 cm^{-1}, respectively. A broad 2D peak is fitted with four Lorenz curve as shown in Figure 1d, which confirms the bilayer graphene. The G and 2D peaks for pristine TLG appears around 1585 and 2707 cm^{-1}, respectively. Figure 1e shows the six Lorenz curve fitting of a broad 2D band of TLG. The absence of D peak in pristine SLG, BLG, and TLG is an indication of defect free high quality graphenes.

Figure 2 shows the Raman spectra of SLG, BLG, and TLG before and after modification of PTSA for different period of time (5, 15, and 30 min). Figure 2a shows the Raman spectra of SLG for different period of time. The intensity of D peak slightly increases after modification with PTSA molecules for different time duration as shown in Figure 2a. However, it does not significantly change with increasing exposure time, which indicates that PTSA molecule has not changed much the graphene lattice structure. The downward shifting of G and 2D

dx.doi.org/10.1021/am401119j | ACS Appl. Mater. Interfaces 2013, 5, 5276−5281

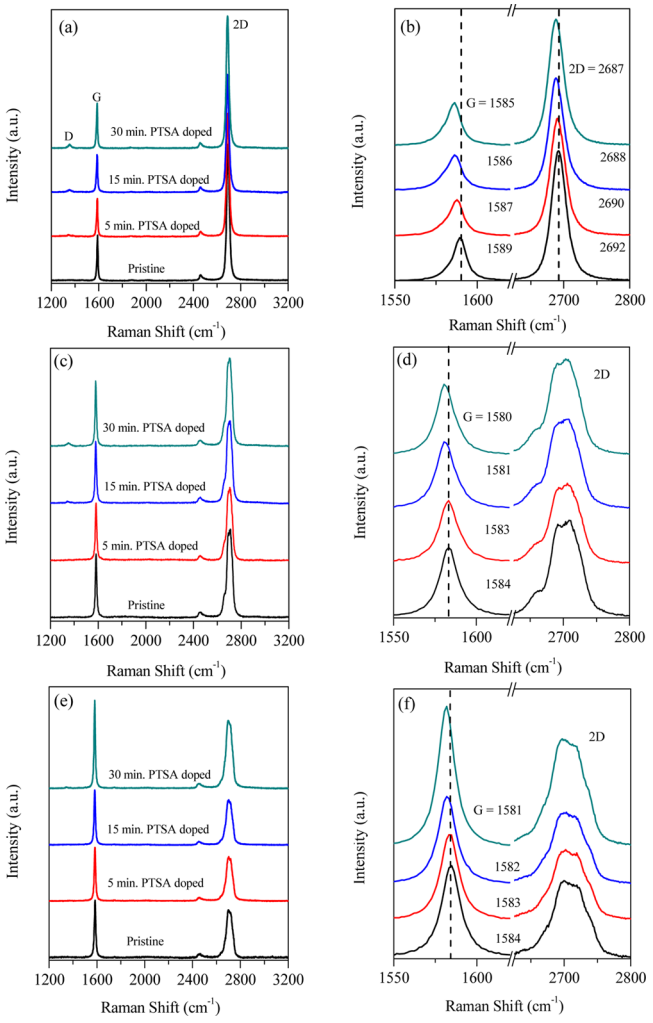

Figure 2. Raman spectra of (a) pristine and PTSA-modified SLG, (b) Raman G and 2D spectra of pristine SLG and PTSA modified SLG, (c) pristine BLG and PTSA modified BLG, (d) Raman G and 2D spectra of pristine BLG and PTSA modified BLG, (e) pristine TLG and PTSA-modified TLG, and (f) Raman G and 2D spectra of pristine TLG and PTSA-modified TLG. The colors coding of panels b, d, and f are same as those in panels a, c, and e, respectively.

peak positions comparing with the pristine single layer graphene is shown in Figure 2b. It is already reported that the shifting of G and 2D peak positions toward lower wavenumber and upper wavenumber is attributed to *n*-type and *p*-type doping, respectively, in SLG.[18,26,27] The shifting of G and 2D peak positions toward lower wavenumber increases with increasing the exposure time.

Figure 2c shows the Raman spectra of BLG for different period of time. The intensity of D peak slightly increases after modification with PTSA molecules for different time duration as shown in Figure 2c. However, the change in the intensity of D peak for BLG is smaller than SLG. The downward shifting of G peak positions is compared to the pristine BLG is shown in Figure 2d. The shifting of G peak position toward lower wavenumber is attributed to *n*-doping of bilayer graphene. Figure 2e shows the Raman spectra of TLG for different period of time. The downward shifting of G peak position in comparison to the pristine TLG is shown in Figure 2f. The shifting of G peak position toward lower wavenumber is also attributed to *n*-doping for trilayer graphene. The shifting of G peak positions is decreased with increasing the number of graphene layers and similarly shifting of G peak positions with thickness were reported for other system.[16] The position of G and 2D of SLG, BLG, and TLG before and after PTSA-doping are summarized in Table 1.

Figure 3a shows I_D/I_G of SLG, BLG, and TLG as function of PTSA exposure time. The I_D/I_G of SLG and BLG increases

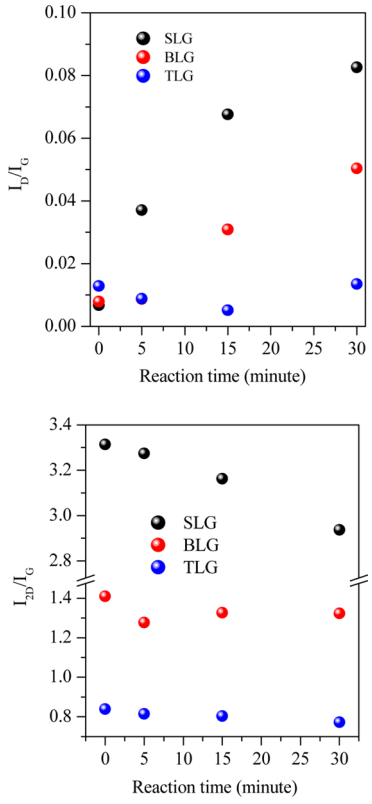

Figure 3. Ratios of the intensities for (a) the D and G peaks and (b) the 2D and G peaks for SLG, BLG, and TLG are plotted as a function of PTSA reaction time.

with increasing PTSA exposure time. However, I_D/I_G of TLG is not significantly changed with PTSA exposure time. The increasing value of I_D/I_G indicates the amount of disorder

Table 1. Raman G and 2D Peak Position and Intensity Ratio of PTSA-Doped SLG, BLG, and TLG

	SLG			BLG			TLG		
samples	G (cm^{-1})	2D (cm^{-1})	I_{2D}/I_G	G (cm^{-1})	2D (cm^{-1})	I_{2D}/I_G	G (cm^{-1})	2D (cm^{-1})	I_{2D}/I_G
pristine	1589	2692	3.3	1584	2708	1.4	1584	2701	0.83
5 min PTSA	1587	2690	3.2	1583	2707	1.2	1583	2700	0.81
15 min PTSA	1586	2688	3.1	1581	2706	1.3	1582	2699	0.80
30 min PTSA	1585	2687	2.9	1580	2705	1.3	1581	2697	0.77

dx.doi.org/10.1021/am401119j | ACS Appl. Mater. Interfaces 2013, 5, 5276−5281

increase with exposure time and also confirms the interaction of PTSA molecules to the graphene layers. However, the effect is small for TLG in comparison to BLG and SLG. Figure 3b shows the intensity ratio of 2D and G peak (I_{2D}/I_G) before and after PTSA treatment for different periods for SLG, BLG, and TLG. The intensity ratio of I_{2D}/I_G are given in Table 1. The ratio of I_{2D}/I_G decreases with increasing the reaction time for all SLG, BLG, and TLG. The reduction in value of I_{2D}/I_G for SLG, BLG, and TLG attributed the doping of PTSA molecule to the various graphene layers. We also observe that the reduction of I_{2D}/I_G decreases significantly with increasing thickness of graphene, indicating that PTSA doping is more effective to the top layer of graphene. Figure 4 shows the 3D atomic force

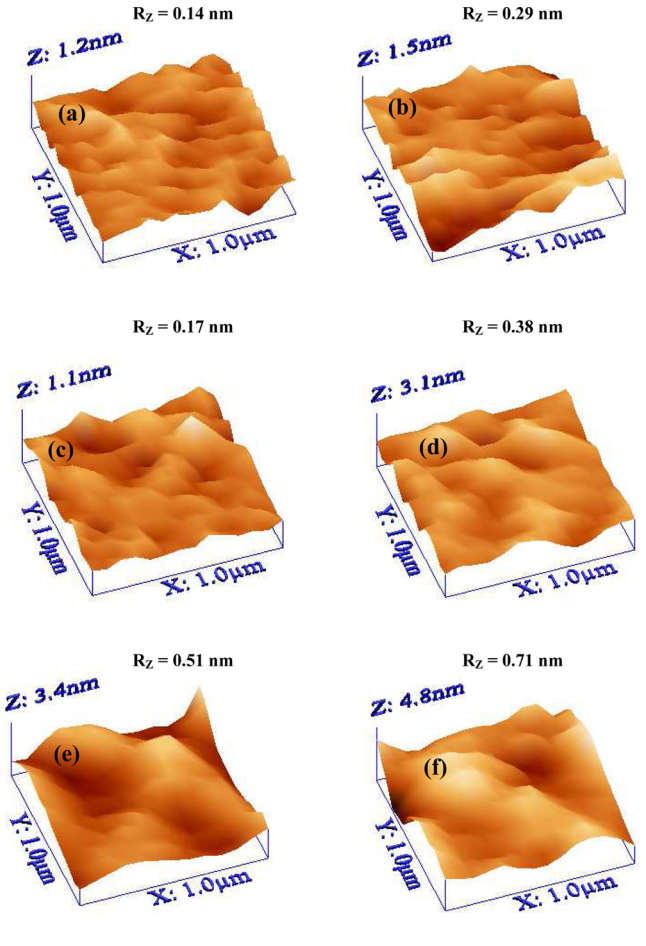

Figure 4. AFM 3D images of (a) pristine SLG, (b) PTSA-doped SLG, (c) pristine BLG, (d) PTSA-doped BLG, (e) pristine TLG, and (f) PTSA-doped TLG.

microscopy (AFM) images of pristine and PTSA-doped (30 min) SLG, BLG, and TLG. Figure 4a and b shows the 3D AFM images of pristine and PTSA-doped SLG. AFM images clearly show the slight change in surface morphology of PTSA doped SLG as compared to pristine SLG. There is also change in root-mean-square roughness (R_z) of pristine and PTSA-doped SLG. R_z increased from 0.14 (pristine) to 0.29 nm (doped) for SLG, from 0.17 (pristine) to 0.38 nm (doped) for BLG, and from 0.51 (pristine) to 0.71 nm (doped) for TLG. The change in roughness is due to the interaction of PTSA molecule to the graphene layers. PTSA molecules interact with carbon lattice of graphene because of the presence of $-SO_3-$ group. It can be also concluded that the nearly constant difference in roughness of pristine and PTSA doped SLG, BLG, and TLG indicates that PTSA molecules were uniformly distributed on various graphene layers. The morphology of exfoliated SLG is different from our previous reported CVD grown SLG. It may be due to the fact that each graphene sample was prepared by two different methods. Obviously CVD prepared graphene even in the intrinsic form is not as much pure as the exfoliated graphene, showing different morphology. In addition, the interaction of PTSA with exfoliated graphene would cause different morphology as compared to the defect contained CVD graphene.

The *n*-doping effect of exfoliated SLG, BLG, and TLG is also confirmed by Dirac point measurements. The resistivity as a function of gate voltage (V_g) before and after PTSA treatment of SLG, BLG, and TLG for different period of time is shown in Figure 5. Figure 5a shows the Dirac point (V_{Dirac}) of SLG for different period of time. The Dirac point (V_{Dirac}) of the pristine SLG is found around V_g = +7 V. The shifting of V_{Dirac} of pristine exfoliated SLG from zero volt (for ideal value) to +7 V is usually caused by atmospheric oxygen, defect introduced during the transferring process, atmospheric moisture, and substrate doping.[28] The shifting of Dirac point toward negative gate voltage indicates the *n*-doping of the exfoliated SLG. The interaction of PTSA molecule and doping with graphene lattice was already explained in our previous paper.[21] Figure 5b and c shows the Dirac point of BLG and TLG respectively, for different period of time. The shift of Dirac points toward negative gate voltage for both BLG and TLG confirmed the *n*-doping. However, the PTSA molecule does not much change the resistivity of the exfoliated SLG, BLG, and TLG at Dirac points. The reason for not significant change in the resistivity of exfoliated SLG, BLG, and TLG at Dirac point may be due to the noncovalent attachment of PTSA molecule to the graphene layers.

Figure 6a shows the changes in charge carrier density (Δn) of SLG, BLG, and TLG as a function of PTSA exposure time. Figure 6a clearly shows the charge carrier density of all SLG, BLG, and TLG are significantly changed after different period of PTSA treatment. The changes in charge carrier density (Δn) of graphene layers were estimated by using the relation $\Delta n = C_g(V_{Dt} - V_{Dp})/e$, where C_g is the gate capacitance ~115 aF/μm^2 for our Si/SiO_2 substrate, V_{Dp} is the Dirac point of pristine SLG, BLG, and TLG, V_{Dt} is the corresponding Dirac point of graphene layers at different PTSA exposure time, and e is the electronic charge. The changes in charge carrier density of graphene layers are related with changes in Fermi level of graphene layers. Thus PTSA-doping significantly modulate the Fermi level of graphene layers. Figure 6b shows the mobility of SLG, BLG, and TLG as a function of the PTSA exposure time. The mobility of the different graphene layers was obtained using relation $\mu = (1/C_g)(\partial\sigma/\partial V_g)$ where σ (1/resistivity) is the conductivity of samples and V_g is the gate voltage. The mobility of pristine and PTSA -doped SLG, BLG, and TLG were calculated on the basis of slope fitted to the linear region of their respective conductivity data. The mobility of SLG slightly decreases with increasing the PTSA exposure time. The slightly reduction in mobility may be due to charge impurities as well as short-range disorders in SLG. However, mobility of BLG and TLG is not much changed with PTSA doping as shown in Figure 6b. The reason for not significant change in mobility of BLG and TLG may be due to interaction of PTSA molecule to the only top layer of BLG and TLG, and then the scattering

dx.doi.org/10.1021/am401119j | ACS Appl. Mater. Interfaces 2013, 5, 5276−5281

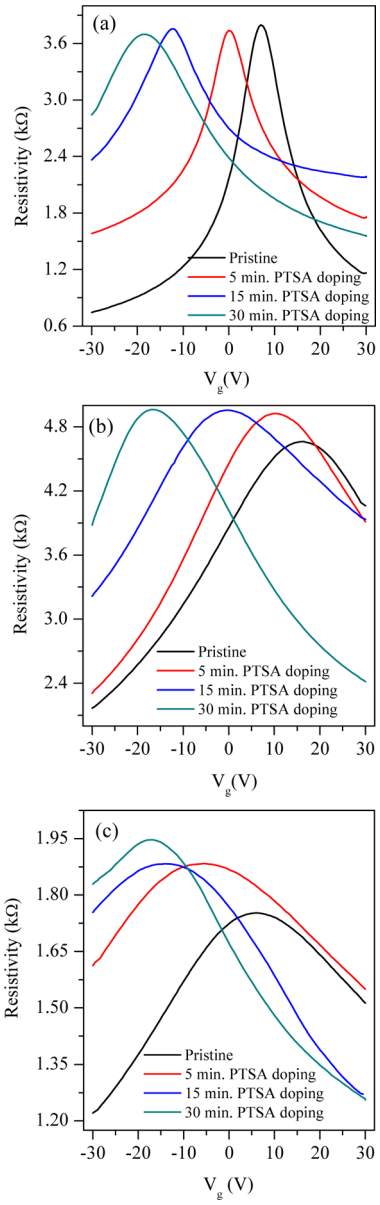

Figure 5. Resistivity as a function of back gate voltage (V_g) for the (a) SLG before and after PTSA treatment for different exposure time, (b) BLG before and after PTSA treatment for different exposure time, and (c) TLG before and after PTSA treatment for different exposure time.

effect due to the charge impurities may be effectively screened by the bottom layer of BLG and TLG in comparison to SLG.

4. CONCLUSION

We have investigated the electrical properties of mechanically exfoliated single-, bi-, and trilayer graphene layers by doping of PTSA molecules. The charge transport and Raman spectroscopy measurements suggest that PTSA molecule imposes the *n*-doping for all single-, bi-, and trilayer graphene layers. The shift of G and 2D peak position and intensity ratios for all single-, bi-, and tri-layer graphene layers are analyzed in terms of reaction time. The reduction in value of I_{2D}/I_G for SLG, BLG, and TLG is attributed to the doping of PTSA molecule to the graphene layers and the reduction of I_{2D}/I_G decreases significantly with increasing thickness of graphene. The shifting of Dirac points after doping of single-, bi-, and trilayer

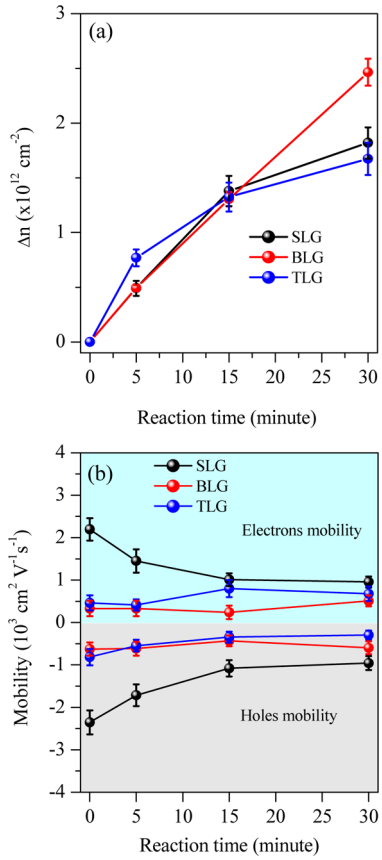

Figure 6. (a) Change in charge density (Δn) as a function of PTSA reaction time for SLG, BLG, and TLG. (b)The electron and hole mobility as a function of PTSA reaction time for SLG, BLG, and TLG.

graphenes toward negative gate voltage also confirmed the *n*-doping. Thus PTSA doping significantly modulates the Fermi level of graphene layers. The results indicate that chemical modification is a simple approach to tailor the electrical properties of graphene layers without degrading electrical properties much. Molecular doping using PTSA is believed to be a feasible scheme for modulating the electronic properties of graphene layers for future graphene-based transparent electronics.

AUTHOR INFORMATION

Corresponding Author

*E-mail: eom@sejong.ac.kr.

Notes

The authors declare no competing financial interest.

ACKNOWLEDGMENTS

This work was supported by Nano-Material Technology Development Program (2012M3A7B4049888) and Priority Research Centers Program (2012-0005859) through the National Research Foundation of Korea (NRF) funded by the Ministry of Education, Science and Technology. This work was also supported by Converging Research Center Program through the Ministry of Education, Science and Technology (2012K001310).

REFERENCES

(1) David, L. H.; Hecht, S.; Irvin, G. *Adv. Mater.* **2011**, *23*, 1482–1513.

(2) Blake, P.; Brimicombe, P. D.; Nair, R. R.; Booth, T. J.; Jiang, D.; Schedin, F.; Ponomarenko, L. A.; Morozov, S. V.; Gleeson, H. F.; Hill, E. W.; Geim, A. K.; Novoselov, K. S. *Nano Lett.* **2008**, *8*, 1704−1708.
(3) Han, T. H.; Lee, Y.; Choi, M. R.; Woo, S. H.; Bae, S. H.; Hong, B. H.; Ahn, J. H.; Lee, T. W. *Nat. Photonics* **2012**, *6*, 105−110.
(4) Park, J. U.; Nam, S. W.; Lee, M. S.; Lieber, C. M. *Nat. Mater.* **2012**, *11*, 120−125.
(5) Geim, A. K.; Novoselov, K. S. *Nat. Mater.* **2007**, *6*, 183−191.
(6) Lu, C. C.; Lin, Y. C.; Yeh, C. H.; Huang, J. C.; Chiu, P. W. *ACS Nano* **2012**, *6*, 4469−4474.
(7) Nair, R. R.; Blake, P.; Grigorenko, A. N.; Novoselove, K. S.; Booth, T. J.; Stauber, T. N.; Peres, M. R.; Geim, A. K. *Science* **2008**, *320*, 1308.
(8) Yan, C.; Cho, J. H.; Ahn, J. H. *Nanoscale* **2012**, *4*, 4870−4882.
(9) Liang, J.; Chen, Y.; Xu, Y.; Liu, Z.; Zhang, L.; Zhao, X.; Zhang, X.; Tian, J.; Huang, Y.; Ma, Y.; Li, F. *ACS Appl. Mater. Interfaces* **2010**, *2*, 3310−3317.
(10) Pang, S.; Hernandez, Y.; Feng, X.; Müllen, K. *Adv. Mater.* **2011**, *23*, 2779−2795.
(11) Forrest, S. R. *Nature* **2004**, *428*, 911−918.
(12) Wu, J.; Agrawal, M.; Becerril, H. A.; Bao, Z.; Liu, Z.; Chen, Y.; Peumans, P. *ACS Nano* **2010**, *4*, 43−48.
(13) Lee, J.; Novoselov, K. S.; Shin, H. S. *ACS Nano* **2011**, *5*, 608−612.
(14) Wang, X. R.; Li, X. L.; Zhang, L.; Yoon, Y.; Weber, P. K.; Wang, H. L.; Guo, J.; Dai, H. J. *Science* **2009**, *324*, 768.
(15) Georgakilas, V.; Otyepka, M.; Bourlinos, A. B.; Chandra, V.; Kim, N.; Kemp, K. C.; Hobza, P.; Zboril, R.; Kim, K. S. *Chem. Rev.* **2012**, *112*, 6156−6214.
(16) Peimyoo, N.; Yu, T.; Shang, J.; Cong, C.; Yang, H. *Carbon* **2012**, *50*, 201−208.
(17) Dong, X.; Long, Q.; Wei, A.; Zhang, W.; Li, L. J.; Chen, P.; Huang, W. *Carbon* **2012**, *50*, 1517−1522.
(18) Shin, H. J.; Choi, W. M.; Choi, D.; Han, G. H.; Yoon, S. M.; Park, H. K.; Kim, S. W.; Jin, Y. W.; Lee, S. Y.; Kim, J. M.; Choi, J. Y.; Lee, Y. H. *J. Am. Chem. Soc.* **2010**, *132*, 15603−15609.
(19) Chen, S. C.; Chang, C. P.; Lee, C. H.; Lin, M. F. *J. Appl. Phys.* **2010**, *107*, No. 083712.
(20) Zhang, Z.; Huang, H.; Yang, X.; Zang, L. *J. Phys. Chem. Lett.* **2011**, *2*, 2897−2905.
(21) Singh, A. K.; Iqbal, M. W.; Singh, V. K.; Iqbal, M. Z.; Lee, J. H.; Chun, S. H.; Shin, K.; Eom, J. *J. Mater. Chem.* **2012**, *22*, 15168−15174.
(22) Zhu, W.; Perebeinos, V.; Freitag, M.; Avouris, P. *Phys. Rev. B* **2009**, *80*, No. 2354021.
(23) Hsu, C. L.; Lin, C. T.; Huang, J. H.; Chu, C. W.; Wei, K. H.; Li, L. J. *ACS Nano* **2012**, *6*, 5031−5039.
(24) Hwang, J.; Choi, H. K.; Moon, J.; Kim, T. Y.; Shin, J. W.; Joo, C. W.; Han, J. H.; Cho, D. H.; Huh, J. W.; Choi, S. Y.; Lee, J. I.; Chu, H. Y. *Appl. Phys. Lett.* **2012**, *100*, No. 133304.
(25) Jo, G.; Choe, M.; Cho, C. Y.; Kim, J. H.; Park, W.; Lee, S.; Hong, W. K.; Kim, T. W.; Park, S. J.; Hong, B. H.; Kahng, Y. H.; Lee, T. *Nanotechnology* **2010**, *21*, 175201−175206.
(26) Kim, K. K.; Reina, A.; Shi, Y.; Park, H.; Li, L. J.; Lee, Y. H.; Kong, J. *Nanotechnology* **2010**, *21*, 285205.
(27) Tongay, S.; Berke, K.; Lemaitre, M.; Nasrollahi, Z.; Tanner, D. B.; Hebard, A. F.; Appleton, B. R. *Nanotechnology* **2011**, *22*, 425701.
(28) Ryu, S.; Liu, L.; Berciaud, S.; Yu, Y. J.; Liu, H.; Kim, P.; Flynn, G. W.; Brus, L. E. *Nano Lett.* **2010**, *10*, 4944−4951.